

Shape-Controlled Silicon Microwire Arrays from Au–Ag-Catalyzed Metal-Assisted Chemical Etching for Radial Junction Solar Cells

Hao Lin,[†] Fei Wu,[†] Pingqi Gao,^{*,‡} and Wenzhong Shen^{*,†}

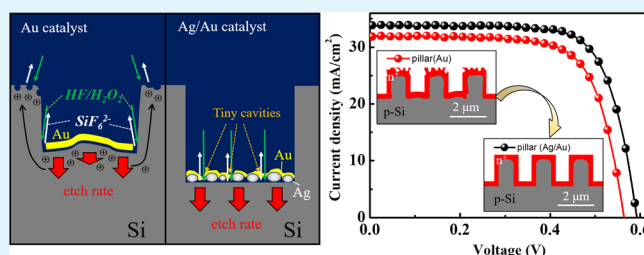
[†]Institute of Solar Energy, and Key Laboratory of Artificial Structures and Quantum Control (Ministry of Education), School of Physics and Astronomy, Shanghai Jiao Tong University, 800 Dong Chuan Road, Shanghai 200240, P. R. China

[‡]School of Materials, Sun Yat-sen University, Guangzhou 510275, P. R. China

Supporting Information

ABSTRACT: Metal-assisted chemical etching (MaCE) has been extensively studied as a cost-effective way to produce silicon nano/micro structure arrays. However, it is hard to keep the resultant morphologies of the nano/micro structures exactly consistent with the original designs because the MaCE process is affected by multiple factors, such as catalyst type, etching solution, temperature, and the interaction with one another. Here, we first proposed an etching model to address the different MaCE behaviors of using Ag, Au, and Ag/Au as catalysts. The model was then independently proven by systematic experiments on the Ag/Au catalyst, with the Au film playing mainly as the frame and the lower Ag film boosting the catalytic activity by increased tiny cavities. With the Ag/Au catalyst, silicon nano/micro arrays with smooth and controllable morphologies from the bottom to the top surface can be successfully formed. Finally, fine-tuned silicon microwire arrays were applied to produce radial junction solar cells, showing a 1.8% increase in absolute efficiency in comparison with the reference cell made by a single metal catalyst. Our findings show that the modified MaCE with Ag/Au catalyst can be an effective way to acquire shape-controlled solar cells with enhanced efficiency.

KEYWORDS: Au–Ag catalysts, metal-assisted chemical etching, silicon microwire arrays, solar cells, radial junction



INTRODUCTION

Owing to their extraordinary properties in optical management, surface wettability, high aspect ratio, and so on, three-dimensional (3D) silicon (Si) nano/micro structure arrays have been widely studied and extensively applied in many areas, such as photovoltaics (PVs), optical devices, biomedicine devices, photoelectrochemical cells, and so on.^{1–6} In terms of the fabrication procedure, solution-based wet etching, especially metal-assisted chemical etching (MaCE), has been successfully demonstrated as an easy-handling and cost-effective way to produce a wide range of 3D Si nano/micro structure arrays.^{7–12} In consideration of the requirements in Si PV, the configurations of the 3D Si nano/micro arrays must be well controlled to balance the gain by light trapping and the loss by surface recombination. For example, tiny nanowire arrays may always suffer from severe surface recombination due to the large surface areas and the excessive defects derived by the catalytic process. While, our recent works showed that radial p–n junction can be more easily formed on the microwires with relatively large diameters (large pitches), upon it both surface and Auger recombination were effectively suppressed.¹³ However, it was found that the uniformity and quality of Si microwire arrays sharply declined with the growth of pitch (distance between adjacent microwires), especially for the pitches larger than 2 μm.^{14,15}

In conventional MaCEs, Ag and Au thin films are two of the most popular catalysts. The Ag film is not chemically stable in etchant solution for Si microwires, and it will be dissolved as the etching process continues running. The morphology of resultant microwires should be varied along with the configuration changes of the Ag films. Thus, the conventional Ag-catalyzed chemical etching is most often used in fabricating random Si nanowires.^{16–19} On the other hand, the Au film is too compact to allow the etchant solution to penetrate effectively, leading to uneven etching at edges (fast) and the central section (slow). This uneven etching will become more prominent with the growth of pattern size and hinder timely refreshment of catalysts because the etchant has to pass through a longer way to reach the middle region. Therefore, to reduce the diffusion length of the etchant, small cavities were always introduced into the basal plane of Au catalyst films by either increasing the evaporation rate or adding tiny sphere patterns.^{14,20} However, silicon nanowires will also be formed during the etching process due to the presence of cavities in the metal films. That is why the reported Si microwire solar cells are always made from reactive-ion etching (RIE).^{6,21,22}

Received: May 21, 2019

Accepted: July 18, 2019

Published: July 18, 2019

To fully boost the merit of MaCE, it is important to find a way to increase the stability of the fabrication process as well as to raise the quality of Si microwire arrays with large pitches. Here, combining the rough property of thin Ag film and the chemical stability of Au, we successfully fabricated a bilayer Ag/Au catalyst film rich with tiny cavities. Meanwhile, etching models for different types of metal catalysts were proposed to understand the advantage of the Ag/Au catalyst in keeping even etch and a smooth top surface. Following that with systematically designed experiments, we further verified the accuracy of the model on the Ag/Au bilayer catalyst film, where the Au film acts as a framework and Ag particles accelerate the etching rate through filling the tiny cavities. With the Ag/Au bilayer film and the help of ethanol, high-quality Si microwire arrays (2.4 μm pitch) were fabricated and continued to construct radial junction solar cells. It showed obvious enhancements among open-circuit voltage (V_{oc}), short-circuit current density (J_{sc}), and efficiency for the Ag/Au catalyst derived solar cell over the one formed solely by the Au catalyst. The modified MaCE method provided here may be beneficial to the shape-controlled Si microwire solar cells.

EXPERIMENTAL SECTION

Fabrication of Silicon Micropillar Arrays. Double-sides polished p-type (100) silicon wafers (1–10 $\Omega\text{-cm}$, 400 μm thick) were utilized in this work. First, 1.2 μm (or 2.4 μm) diameter monolayer polystyrene (PS) spheres were deposited on the wafers through the Langmuir–Blodgett (LB) method,²³ and then the diameter of spheres was reduced to around 1.0 μm (or 2.0 μm) by reactive-ion etching (RIE) through adjusting the etching time with fixed O_2 flow at 60 sccm and power at 60 W. Here the etching times for 1.2 μm -PS (or 2.4 μm -PS) are 45 s (or 90 s). Second, metal films, such as the adhesive layer of 0.5 nm Ti and catalyst films of Au or Ag/Au, were deposited sequentially on the PS spheres side by using electron beam evaporation (E-beam) with a deposition rate of 0.5 $\text{\AA}/\text{s}$. Third, PS spheres were removed by chloroform with sonication, and metal mesh will be formed on the wafers. At last, the samples were immersed in the etching solution at room temperature, and then the pillar structure can be achieved via this metal-assisted chemical etching. In this study, the etching solution of the traditional method is $\text{HF}/\text{H}_2\text{O}_2/\text{H}_2\text{O} = 5/1/20$ by volume, while that of the modified method is $\text{HF}/\text{H}_2\text{O}_2/\text{EtOH}/\text{H}_2\text{O} = 5/1/10/10$ by volume. The concentrations of HF and H_2O_2 are ~ 4.8 and ~ 0.4 M, respectively, and EtOH is ethanol. The micropencil arrays were fabricated by a multiple-cycle chemical etching process, and more details can be found in the previous publication.²⁴

Fabrication of Silicon Photovoltaic Devices. It is noted that a planar region on the wafer surface was retained to carry on the later processing step of depositing top electrodes ($\sim 10\%$ areas in total front surface of device). As reported by our previous paper,²⁵ this was achieved by a photolithography protection and then exposed the rest of the surface for fabricating corresponding pillar textures by using the above-mentioned methods (fabrication of silicon micropillar arrays). After that, the metal mesh was removed by aqua regia, following which the samples were cleaned by the standard RCA process,²⁶ and then an indirect doping method¹³ with spin-on dopant (SOD) was used to form the emitter layer on the surface of the pillar structure. The whole diffusion process was implemented under the atmosphere of O_2 (375 sccm) and N_2 (1125 sccm) for 30 min, and the diffusion temperature was fixed at 850 $^\circ\text{C}$. This diffusion process produced a thin phosphorosilicate glass (PSG) layer with a quite uniform thickness of 30–40 nm on the surface of silicon.¹³ This PSG layer was directly served as a passivation layer, showing a satisfied passivation quality. After that, back metal contact was formed by printing aluminum paste on the rear side of the devices and following an alloying process at 750 $^\circ\text{C}$. Photoresist patterns were then fabricated by the photolithography method for deposition of the top electrode.

Finally, the PSG layer exposed by the photoresist patterns was totally removed by using 10 wt % HF solution, and the top electrode (Cr/Pd/Ag) was fabricated by using the deposition and lift-off process.

Characterization. The morphologies of the samples were conducted by a scanning electron microscope (SEM, Zeiss Ultra Plus). Light J - V of solar cells was measured under a simulated AM 1.5 spectrum sunlight illumination and with an 0.5 cm^2 effective illumination area through a measurement mask. External quantum efficiency (EQE) and reflectance spectra were measured by a quantum efficiency system (QEX10).

RESULTS AND DISCUSSION

First, let us review the basic principle of MaCE.¹² It is a catalytic process with accelerated reduction/oxidation reaction at the interface between silicon and metal catalysts. The reduction reaction on oxidant (here is H_2O_2) catalyzed by a metal film will generate and inject holes into the silicon surface. The silicon near the interface of metal/silicon is then oxidized by the holes and dissolved by HF. The etching rate is thus determined by the diffused holes, and therefore it will be much faster at the metal/silicon interface than the bare silicon portions without metal coverage. That means the shape of silicon textures may mainly depend on the pattern configuration of the metal catalyst. For example, in our experiment, the Au mesh arrays will produce pillar arrays.

However, the etching results do not always straightforwardly follow the initial patterns, whereas the etching shapes show a high dependence on the employed metal catalysts. As shown in Figure 1, the top-view SEM images of different catalyst films

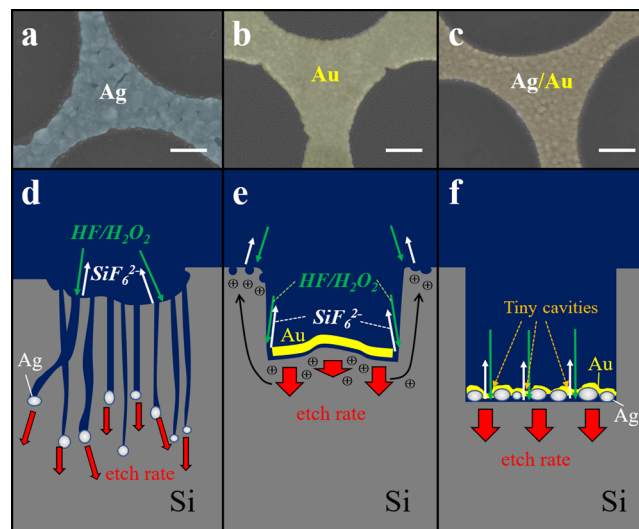


Figure 1. Top-view SEM images of different catalyst films (a–c) and corresponding etching models (d–f) of MaCE: 20 nm Ag film (a, d), 20 nm Au film (b, e), and 5/10 nm Ag/Au bilayer film (c, f). All scale bars in the SEM images are 200 nm.

(a–c) and the corresponding mechanism models (d–f) were tentatively presented to explain the difference. Actually, a thin Ti film was inserted as an adhesive layer between the metal catalysts and silicon surface. Because the Ti will be easily dissolved by HF during the etching process, it is convenient to only mark the components of catalysts while omitting Ti in the following description. First, we discuss the situation of the Ag catalyst. It is well-known that Ag has a better chemical activity and will be slowly dissolved in the $\text{HF}/\text{H}_2\text{O}_2$ etching solution. As a consequence, the Ag film will gradually become isolated

Ag particles during the etching process, leading to the appearance of Si nanowires between adjacent microwires (see Figure 1d). Compared with Ag, the Au film has not only good chemical stability but also good continuity, so the Au film would be kept as a whole during the etching process. However, an inherently negative effect of the compact Au film is the difficulty of penetrating the etchant (Figure 1b), leading to a nonuniform distribution of fresh etching solution at the metal/silicon interface during etching process. This will result in uneven etching, where the etching rate at the edge of Au pattern is much higher than that at the center (Figure 1e). More importantly, this difference of etch rate will be passed on to the final etching configuration. Meanwhile, at the Au/Si interface, because of the difficulty of exchanging etching solution, the oxidation of silicon and the consumption of injected holes will be slowed down. That means a number of excess holes will diffuse from the Au/Si interface to the top surface of the microwire and then etch the silicon and form a nanopore structure (see the top part of silicon in Figure 1e). In other words, the compact property of the Au film partially hinders the etching reaction of silicon at the Au/Si interface and transfers a part of the etching reaction of silicon to the top surface of the microwire, resulting in a rough top surface. For the situation of the Ag/Au bilayer film, as shown in Figure 1c, it is not as compact as the Au film, and the surface becomes more rough. This indicates that there should exist amounts of tiny cavities on the metal film, which will largely increase the penetration of etching solution, facilitating quick exchange of etching solution and uniform etching. Therefore, after using Ag/Au bilayer as catalyst, we can expect to obtain high quality silicon microwire arrays with a flat bottom plane and a smooth top surface (Figure 1f).

As shown in Figure 2, we exhibit the etching results with the traditional method (Figure 2a–c) and the modified method

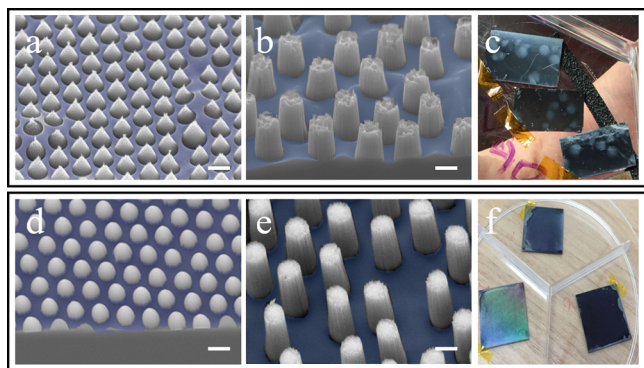


Figure 2. Comparison of etching results from traditional Au catalyst (a–c) and modified Ag/Au bilayer catalyst (d–f). SEM images of (a, d) a micropencil with 1.2 μm pitch on polished silicon wafer, (b, e) a micropillar with 2.4 μm pitch on polished silicon wafer, and (c, f) photo images of micropencil with 1.2 μm pitch on a polished silicon wafer. All scale bars in the SEM images are 1 μm .

(Figure 2d–f). Here the traditional method refers to Au as the metal catalyst and $\text{HF}/\text{H}_2\text{O}_2/\text{H}_2\text{O}$ solution as the etchant, while the modified method uses Ag/Au as the metal catalyst and $\text{HF}/\text{H}_2\text{O}_2/\text{EtOH}/\text{H}_2\text{O}$ solution as the etchant. Here, the purpose of adding EtOH in the modified method is to eliminate the blebs engendered from the reaction. Figures 2b and 2e are 2.4 μm pitch arrays, while others samples in Figures 2a, 2d, 2c, and 2f are 1.2 μm pitch arrays. From the SEM

images, we can clearly find that with the increase of pitch from 1.2 to 2.4 μm the flatness of the array's bottom plane (blue color) becomes worse in the traditional method, while that in the modified method remains smooth. Meanwhile, the top surface of 2.4 μm pitch microwire arrays in the modified method (Figure 2e) is also obviously smoother than that in the traditional method (Figure 2b). In Figures 2c and 2f, we also exhibited examples of achieving 1.2 μm pitch micropencils with different etching methods. From that, white spots and color differences appear in the traditional method, while they are not found in the samples from the modified method. That indicates the modified etching method can produce uniform pillar structures with smoother surface over the whole sample scale. Therefore, from above experiments, the mechanism models shown in Figures 1e and 1f were well proven.

To further understand the difference among them, SEM images of the catalyst films after the etching process are shown in Figure 3. The Au film is still compact and smooth (Figure

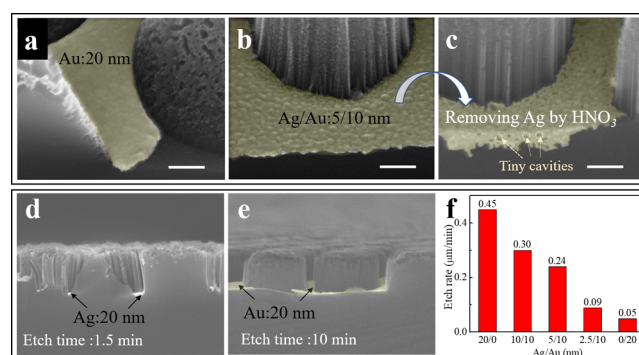


Figure 3. (a–c) SEM images of different metal films after MaCE process: (a) 20 nm Au film, (b) 5/10 nm Ag/Au bilayer film, and (c) the remained Au film after removing Ag by HNO_3 . (d–f) The measurements of etching rate. Cross-sectional SEM images for measuring the etching rate of MaCE with different metal films: (d) 20 nm Ag film and (e) 20 nm Au film. (f) Etching rate of MaCE with different metal films at room temperature. All scale bars are 200 nm.

3a), while the Ag/Au bilayer film is relatively rough (Figure 3b). After using HNO_3 to remove Ag component in the Ag/Au bilayer film (Figure 3c), we can clearly see the tiny cavities of the Au film (Figure 3c), manifesting the accuracy of the mechanism model in Figure 1f. In addition, to only study the influence of metal catalyst to the etching rate, in the following experiments, the same etching solution ($\text{HF}/\text{H}_2\text{O}_2/\text{EtOH}/\text{H}_2\text{O} = 5/1/10/10$ by volume) was used. According to the cross-sectional SEM image in Figures 3d, 3e, and 4f–h, the etching rate of MaCE with different catalyst films can be calculated, as shown in Figure 3f. It shows that the 20 nm Ag film (the first bar in Figure 3f) has the largest etching rate up to 0.45 $\mu\text{m}/\text{min}$. However, the resultant morphology by the Ag catalyst becomes noticeably worse, and the amounts of the nanowire structure were presented between each adjacent microwire (Figure 3d). In contrast, the 20 nm Au film (the rightmost bar) has the lowest etching rate of down to 0.05 $\mu\text{m}/\text{min}$, but the microwire morphology produced is relatively better than that from the Ag film. The Ag/Au bilayer films have a moderate etching rate of in between the values of pure Au and pure Ag. With the decrease of the Ag/Au ratio, the etching rate will be reduced. For example, the etching rate was found to decrease from 0.30 $\mu\text{m}/\text{min}$ for 10 nm Ag/10 nm Au to 0.09 $\mu\text{m}/\text{min}$ for 2.5 nm Ag/10 nm Au.

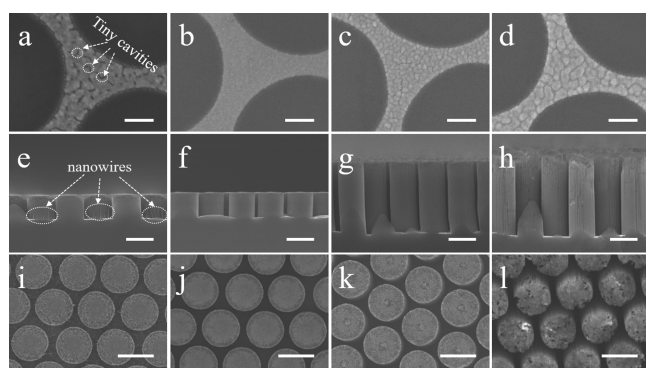


Figure 4. Top-view SEM images of Ag/Au bilayer film (a–d); corresponding cross-sectional (e–h) and top-view SEM images (i–l) of the etched Si microwire arrays. The thickness of Ag/Au is (a, e, i) 0/13 nm, (b, f, j) 2.5/10 nm, (c, g, k) 5/10 nm, and (d, h, l) 10/10 nm, respectively. Scale bars are 200 nm in (a–d) and 1 μm in (e–l).

To clearly understand the main functions of Ag and Au in Ag/Au bilayer film, the reaction results from the Ag/Au catalysts with varied thickness were examined. Figure 4 shows the top-view SEM images of the Ag/Au film with a varied thickness on the silicon wafer and the corresponding morphology of resultant microwire arrays (including cross-sectional and top-view SEM images after 10 min etching). From Figure 4a, one can see that the Au film can also form tiny cavities when its thickness was reduced from 20 to 13 nm. With the help of tiny cavities, the bottom surface of silicon arrays produced by 13 nm Au is much flatter than the 20 nm Au film (Figure 3e), except for a large number of tiny nanowires between adjacent microwires. Meanwhile, the top surface of the 13 nm Au derived microwires is still slightly worse than the situation in Figures 4f and 4j, in which the metal films contain 2.5/10 nm Ag/Au. Then, we further studied the influence of the Ag film thickness in the Ag/Au bilayer film, where we fixed the thickness of Au as 10 nm. From Figures 4b–d and 4f–h, the roughness of the Ag/Au bilayer film and the etching rate will increase with the growth of the Ag film thickness. Meanwhile, in comparison to the

morphology of the top surface, as shown in Figures 4k,l, it shows the roughness will become very important once the Ag film is thicker than 10 nm. This is because the Au film is too thin to well cover the thick Ag particles, facilitating the dissolution and deposition of Ag on the top surface of the structures through the redox reaction and then forming new nucleation sites for etching. Therefore, considering the quality and the etching rate, one optimized thickness of the Ag film is 5 nm. From the above studies, we concluded that the Au film mainly plays the role of a frame, while Ag increases the tiny cavities of bilayer films for realizing effective penetration of etching solution and improving etching uniformity and catalytic activity.

After well studying the difference of etching results caused by different metal catalysts, we applied the pillar textures to photovoltaics, as shown in Figure 5. Because only the Au catalyst is difficult to fabricate silicon micropillar arrays with a large pitch, we chose the 2.4 μm pitch pillar as the object in this application. The schematic of Si microwire solar cells is shown in Figure 5a. Note that the Si surface beneath the top electrodes was not textured and always maintained a planar state, which is beneficial for good contacts and better conductivity. Details about how to reserve the planar surface for metallization can be found in our previous paper.²⁵ Figures 5b and 5c show the SEM images of pillar arrays fabricated by a single Au metal catalyst and Ag/Au catalyst, respectively. The pillar structure fabricated by the Ag/Au film is smoother than that by the Au film, especially the top surface of pillar (see the insets). The corresponding PV performances are shown in Figure 5d and Table 1. To have a reference, we added a planar solar cell with the same fabricating process in them. Even the efficiencies of our solar cells are still not high enough considering the immature manufacture and large shaded area of the top electrodes; the results give obvious trends of different structures. Through use of the Ag/Au bilayer film as catalyst, V_{oc} , J_{sc} , and η all have a large increase, from 564 mV, 31.9 mA/cm^2 , and 12.8% of the Au film case to 593 mV, 33.9 mA/cm^2 , and 14.6%, respectively. The V_{oc} of pillar (Ag/Au) solar cells is very close to that of planar ones, indicating a good

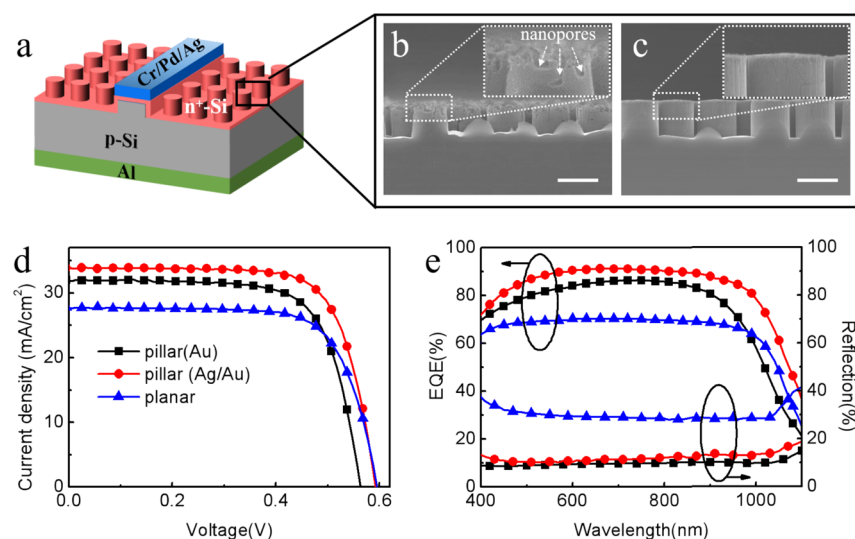


Figure 5. Comparison of pillar textures with different methods in Si solar cells. (a) Schematic illustration of pillar textured solar cell. (b, c) SEM images of 2.4 μm pitch silicon micropillar arrays fabricated by 20 nm Au film as catalyst (b) and 5/10 nm Ag/Au films as catalyst (c). (d) Light J – V curves and (e) EQE as well as reflection spectra for the three kinds of devices. All scale bars in the SEM images are 2 μm .

Table 1. Photovoltaic Performances of the Silicon Solar Cells in Figure 5d

samples ^a	V_{oc}^b (V)	J_{sc}^b (mA/cm ²)	FF ^b (%)	PCE ^b (%)
pillar (Au)	0.564 (0.557 ± 0.008)	31.9 (31.9 ± 0.1)	71.0 (69.3 ± 1.4)	12.8 (12.3 ± 0.4)
pillar (Ag/Au)	0.593 (0.586 ± 0.005)	33.9 (33.8 ± 0.1)	72.8 (72.5 ± 0.4)	14.6 (14.4 ± 0.2)
planar	0.595 (0.593 ± 0.004)	27.7 (27.4 ± 0.4)	72.0 (72.5 ± 0.6)	11.9 (11.8 ± 0.1)

^aData and statistics based on five cells of each condition. ^bNumbers in bold are the champion values of each condition.

passivation on the surface of pillar (Ag/Au) structure. That can also well be proven by measuring the dark saturation current density (J_0) and minority carrier lifetime through passivation samples (more details are shown in Figures S1 and S2). Pillar (Au) has the highest J_0 , ~800 fA/cm², while J_0 for pillar (Ag/Au) and planar Si are 300 and 85 fA/cm², respectively. For the minority carrier lifetime, pillar (Ag/Au) and planar Si both are ~220 μ s, which is twice as large as that of pillar (Au). This result does indicate that a bilayer of Ag/Au catalyst can fabricate a higher quality pillar structure, which is a crucial step to obtain high quality passivation. Anyway, on the basis of one example of using passivation strategy combining diffused N⁺-Si layer and PSG layer, we have proven the pillar array from the Ag/Au catalyst can render a passivation level even comparable to the planar Si wafer. At the same time, we also exhibit the corresponding EQE and reflection spectra in Figure 5e. From the reflection spectra, the planar structure has the highest reflection (>30%) over the whole spectrum, while the reflection of pillar structures is only ~11%. It should be noted that the reflection of pillar (Au) is slightly lower than that of pillar (Ag/Au) due to the presence of nanopores on the top surface of pillar (Au). However, because of the nanopore's structure, it will also increase the surface area of the original pillar structure, which may be the main reason leading to the worst passivation of pillar (Au). More importantly, with the formation of nanopores structure on the top parts of pillars, it will increase the real doping depth of this region. That will lead to the increase of Auger recombination.^{13,18} Therefore, at last, pillar (Ag/Au) has a higher EQE compared with that of pillar (Au).

It is well-known that a damaged layer enriched with defects will be produced at the surface of nano/micro structure in all fabrication methods, including MaCE using pure Ag catalyst, the dry-etching method, and our MaCE using Ag/Au catalyst. However, the thickness of the damaged layer is different. The first two methods will produce a thicker damaged layer, especially the first one due to the chemical instability of Ag. Therefore, for the as-fabricated Si nanostructures, it is a common way to improve their quality by using post chemical treatments to partially remove the damaged layer.¹⁶ Compared with MaCE with Ag catalyst, our Ag/Au bilayer film can well limit the dissolution of Ag and largely reduce the thickness of damaged layer. More importantly, from the measurement of the lifetime in Figure S2, we can see the lifetime of pillar (Ag/Au) is nearly close to that of planar Si wafer (without damaged layer), reaching ~220 μ s. That indicates the damaged layer in our method can be well controlled, and it nearly does not affect the surface passivation quality. All the results showed above indicate that the MaCE with Ag/Au bilayer catalyst could be an effective way to produce high quality micropillars with highly suppressed surface and Auger recombination.

CONCLUSION

In summary, a modified metal-assisted chemical etching method with Ag/Au bilayer catalyst was presented to

successfully produce high quality (including flat bottom surface, smooth top surface, and uniform height) silicon micropillar arrays. The mechanism models of different metal catalysts were analyzed and then confirmed through systematic experiments. It proven that the Au film in the Ag/Au bilayer mainly plays the role of frame while Ag can accelerate the etching process by increasing tiny cavities through the bilayer film. With the help of tiny cavities, the effective penetration of etching solution was realized in the bilayer film, which increases the etching uniformity. Finally, we applied pillar textures with traditional and modified methods to photovoltaics, showing a champion efficiency of 14.6% for the solar cells from modified method and 12.8% for the one from traditional method. It indicates that the modified MaCE method can obtain a high quality of silicon pillar arrays for shape-controlled solar cells.

ASSOCIATED CONTENT

Supporting Information

The Supporting Information is available free of charge on the ACS Publications website at DOI: 10.1021/acsam.9b01006.

Characterization of the passivation quality, including dark saturation current density (J_0) and minority carrier lifetime (PDF)

AUTHOR INFORMATION

Corresponding Authors

*E-mail: gaopq3@mail.sysu.edu.cn.

*E-mail: wzshen@sjtu.edu.cn.

ORCID

Pingqi Gao: 0000-0002-6424-4835

Notes

The authors declare no competing financial interest.

ACKNOWLEDGMENTS

This work was supported by the Major State Basic Research Development Program of China (No. 2018YFB1500302 and No. 2016YFB0700700), National Natural Science Foundation of China (11674225, 11834011, 11474201, 61674154, and 61874177), and Zhejiang Provincial Natural Science Foundation (LR19E020001 and LR16F040002). We thank the Center for Advanced Electronic Materials and Devices (AEMD) of Shanghai Jiao Tong University for supplying the facility of reactive-ion etching (RIE).

REFERENCES

- (1) Wang, X.; Liu, Z.; Yang, Z.; He, J.; Yang, X.; Yu, T.; Gao, P.; Ye, J. Heterojunction Hybrid Solar Cells by Formation of Conformal Contacts between PEDOT:PSS and Periodic Silicon Nanopyramid Arrays. *Small* **2018**, *14* (15), 1704493.
- (2) Yamada, K.; Yamada, M.; Maki, H.; Itoh, K. M. Fabrication of arrays of tapered silicon micro-/nano-pillars by metal-assisted chemical etching and anisotropic wet etching. *Nanotechnology* **2018**, *29* (28), 28LT01.

- (3) Hamdana, G.; Südkamp, T.; Descoins, M.; Mangelinck, D.; Caccamo, L.; Bertke, M.; Wasisto, H. S.; Bracht, H.; Peiner, E. Towards fabrication of 3D isotopically modulated vertical silicon nanowires in selective areas by nanosphere lithography. *Microelectron. Eng.* **2017**, *179*, 74–82.
- (4) Diederichs, T.; Nguyen, Q. H.; Urban, M.; Tampé, R.; Tornow, M. Transparent nanopore cavity arrays enable highly parallelized optical studies of single membrane proteins on chip. *Nano Lett.* **2018**, *18* (6), 3901–3910.
- (5) Lee, K.; Hwang, I.; Kim, N.; Choi, D.; Um, H. D.; Kim, S.; Seo, K. 17.6%-Efficient radial junction solar cells using silicon nano/micro hybrid structures. *Nanoscale* **2016**, *8* (30), 14473–9.
- (6) Hwang, I.; Um, H.-D.; Kim, B.-S.; Wober, M.; Seo, K. Flexible crystalline silicon radial junction photovoltaics with vertically aligned tapered microwires. *Energy Environ. Sci.* **2018**, *11* (3), 641–647.
- (7) Liu, Y.; Zi, W.; Liu, S.; Yan, B. Effective light trapping by hybrid nanostructure for crystalline silicon solar cells. *Sol. Energy Mater. Sol. Cells* **2015**, *140*, 180–186.
- (8) Li, M.; Li, Y.; Liu, W.; Yue, L.; Li, R.; Luo, Y.; Trevor, M.; Jiang, B.; Bai, F.; Fu, P.; Zhao, Y.; Shen, C.; Mbengue, J. M. Metal-assisted chemical etching for designable monocrystalline silicon nanostructure. *Mater. Res. Bull.* **2016**, *76*, 436–449.
- (9) Bai, F.; Zhang, Y.; Duan, Z.; Hoye, R.; Trevor, M.; Li, Y.; Li, M. Broadband antireflection property of silicon nanocone arrays with porous sidewalls fabricated by Ag-catalyzed etching. *AIP Adv.* **2017**, *7* (9), 095006.
- (10) Venkatesan, R.; Arivalagan, M. K.; Venkatachalapathy, V.; Pearce, J. M.; Mayandi, J. Effects of silver catalyst concentration in metal assisted chemical etching of silicon. *Mater. Lett.* **2018**, *221*, 206–210.
- (11) Li, L.; Tuan, C.-C.; Zhang, C.; Chen, Y.; Lian, G.; Wong, C.-P. Uniform Metal-Assisted Chemical Etching for Ultra-High-Aspect-Ratio Microstructures on Silicon. *J. Microelectromech. Syst.* **2019**, *28* (1), 143–153.
- (12) Huang, Z.; Geyer, N.; Werner, P.; de Boor, J.; Gosele, U. Metal-assisted chemical etching of silicon: a review. *Adv. Mater.* **2011**, *23* (2), 285–308.
- (13) Wu, F.; Lin, H.; Yang, Z.; Liao, M.; Wang, Z.; Li, Z.; Gao, P.; Ye, J.; Shen, W. Suppression of surface and Auger recombination by formation and control of radial junction in silicon microwire solar cells. *Nano Energy* **2019**, *58*, 817–824.
- (14) Lin, H.; Fang, M.; Cheung, H.-Y.; Xiu, F.; Yip, S.; Wong, C.-Y.; Ho, J. C. Hierarchical silicon nanostructured arrays via metal-assisted chemical etching. *RSC Adv.* **2014**, *4* (91), 50081–50085.
- (15) Yan, J.; Wu, S.; Zhai, X.; Gao, X.; Li, X. Facile fabrication of wafer-scale, micro-spacing and high-aspect-ratio silicon microwire arrays. *RSC Adv.* **2016**, *6* (90), 87486–87492.
- (16) Leontis, I.; Botzakaki, M. A.; Georga, S. N.; Nassiopoulou, A. G. Study of Si Nanowires Produced by Metal-Assisted Chemical Etching as a Light-Trapping Material in n-type c-Si Solar Cells. *ACS Omega* **2018**, *3*, 10898–10906.
- (17) Huang, Z.; Song, X.; Zhong, S.; Xu, H.; Luo, W.; Zhu, X.; Shen, W. 20.0% Efficiency Si Nano/Microstructures Based Solar Cells with Excellent Broadband Spectral Response. *Adv. Funct. Mater.* **2016**, *26* (12), 1892–1898.
- (18) Oh, J.; Yuan, H. C.; Branz, H. M. An 18.2%-efficient black-silicon solar cell achieved through control of carrier recombination in nanostructures. *Nat. Nanotechnol.* **2012**, *7* (11), 743–8.
- (19) Wang, Z.; Peng, S.; Wen, Y.; Qin, T.; Liu, Q.; He, D.; Cao, G. High-Performance Si/Organic Hybrid Solar Cells using A Novel Cone-shaped Si Nanoholes Structures and Back Surface Passivation Layer. *Nano Energy* **2017**, *41*, 519–526.
- (20) Um, H. D.; Kim, N.; Lee, K.; Hwang, I.; Hoon Seo, J.; Yu, Y. J.; Duane, P.; Wober, M.; Seo, K. Versatile control of metal-assisted chemical etching for vertical silicon microwire arrays and their photovoltaic applications. *Sci. Rep.* **2015**, *5*, 11277.
- (21) Ro, Y. G.; Chen, R.; Liu, R.; Li, N.; Williamson, T.; Yoo, J.; Sim, S.; Prasankumar, R. P.; Dayeh, S. A. Surface Passivation and Carrier Collection in {110}, {100} and Circular Si Microwire Solar Cells. *Adv. Energy Mater.* **2018**, *8* (33), 1802154.
- (22) Elbersen, R.; Vijselaar, W.; Tiggelaar, R. M.; Gardeniers, H.; Huskens, J. Effects of Pillar Height and Junction Depth on the Performance of Radially Doped Silicon Pillar Arrays for Solar Energy Applications. *Adv. Energy Mater.* **2016**, *6* (3), 1501728.
- (23) Gao, P.; He, J.; Zhou, S.; Yang, X.; Li, S.; Sheng, J.; Wang, D.; Yu, T.; Ye, J.; Cui, Y. Large-Area Nanosphere Self-Assembly by a Micro-Propulsive Injection Method for High Throughput Periodic Surface Nanotexturing. *Nano Lett.* **2015**, *15* (7), 4591–8.
- (24) Lin, H.; Cheung, H.-Y.; Xiu, F.; Wang, F.; Yip, S.; Han, N.; Hung, T.; Zhou, J.; Ho, J. C.; Wong, C.-Y. Developing controllable anisotropic wet etching to achieve silicon nanorods, nanopencils and nanocones for efficient photon trapping. *J. Mater. Chem. A* **2013**, *1* (34), 9942.
- (25) Liang, X.; Shu, L.; Lin, H.; Fang, M.; Zhang, H.; Dong, G.; Yip, S.; Xiu, F.; Ho, J. C. Inverted Silicon Nanopencil Array Solar Cells with Enhanced Contact Structures. *Sci. Rep.* **2016**, *6*, 34139.
- (26) Tong, H.; Yang, Z.; Wang, X.; Liu, Z.; Chen, Z.; Ke, X.; Sui, M.; Tang, J.; Yu, T.; Ge, Z.; Zeng, Y.; Gao, P.; Ye, J. Dual functional electron-selective contacts based on silicon oxide/magnesium: tailoring heterointerface band structures while maintaining surface passivation. *Adv. Energy Mater.* **2018**, *8* (16), 1702921.